Effects of Uncertainty in Gas-Surface Interaction on DSMC Simulations of Hypersonic Flows

Marat Kulakhmetov, A. Venkattraman, and Alina A. Alexeenko

School of Aeronautics and Astronautics, Purdue University, West Lafayette, IN 47907, USA

Abstract. This study uses the non-intrusive generalized polynomial chaos method to investigate the effects of uncertainties in the gas-surface interaction model on the hypersonic boundary layer flow over a flat plate. In particular, the polynomial chaos method is applied to assess uncertainties in the surface shear, normal stress, heat flux, flowfield temperature and density resulting from uncertain surface temperature and accommodation coefficient. The polynomial chaos approach allows us to estimate probability density functions from fewer flowfield samples than the traditional random Monte Carlo sampling. The flowfield solutions are computed by the DSMC code SMILE. The analysis shows that surface fluxes and flowfields in the hypersonic boundary layer are more sensitive to the accommodation coefficient than surface temperature uncertainty.

Keywords: Gas-Surface Interaction, Hypersonic Aerothermodynamics, Uncertainty Quantification.
PACS: 51.10.+y

INTRODUCTION

The development of advanced hypersonic aerospace vehicles requires prediction of hypersonic flows and aeroheating with a high degree of confidence.[1] The uncertainties in the hypersonic flow predictions stem from the variability in flight conditions, e.g. freestream and material properties, as well as from a lack of adequate models for the complex physico-chemical processes occurring in the high-enthalpy environment of hypersonic flight.[2] Gas-surface interactions in hypersonic boundary layers involve a complex mass, momentum and energy coupling between the gaseous and solid phases that are often approximated by simplified gas-surface interaction models. The uncertainties in the model form and parameters of gas-surface interactions can potentially be a source of large overall deviations between computational predictions and flight data. Here we study the effects of uncertainties in gas-surface interaction parameters on the hypersonic boundary layer flowfield and surface properties.

Thermal and chemical non-equilibrium are distinguishing features of hypersonic flows. Because of the strong effects of non-equilibrium, the direct simulation Monte Carlo (DSMC) method is often employed for hypersonic flow simulations. Typical DSMC simulations have significantly higher computational costs compared to CFD. Until recently, the most widely used approach for UQ analysis has been the random Monte Carlo sampling that usually involves generation of hundreds or thousands of flowfield solutions samples. The large sample size and the presence of statistical noise in a DSMC solution make such Uncertainty Quantification (UQ) analyses impractical. Here we apply the generalized polynomial chaos expansion (gPC) method [3,4] based on deterministic sampling of DSMC solutions.

The third-order gPC expansion with a third-order Gaussian quadrature requires only three DSMC solutions and allows us to construct the first three moments of the distribution function of the output parameters of interest. The analysis by Weaver et al [5] shows that 3rd order gPC can accurately reproduce (within 0.1%) the first two moments, i.e. the mean and the standard deviation, of the surface heating and stresses for typical hypersonic flows of non-reacting gas. A typical gPC expansion for an output variable, y, at location, x, and with a test random variable, z, is presented in Eq. 1. The orthogonal polynomials, ψ_n, in gPC are chosen such that their orthogonal weights are equivalent to the distribution function, $\rho(z)$, of the random variable, z. Since this study considers only a 3rd order expansion with uniform random variable distributions, Eq.1 is truncated at N = 2 and ψ_n are Legendre polynomials, which can be found in table 1.

gPC weights, a_n, can be computed by multiplying Eq. 1 by ψ_m, computing expectations of both sides and rearranging, as shown on the left side in Eq.2 . Due to the orthogonality of Legendre polynomials, $<\psi_{m*}\psi_n>$ equals to zero if m≠n. Since there is no known closed form relationship between z and y the expectation $<y\ \psi_n>$ in Eq.2 has to be evaluated numerically. Although it is possible to compute this expectation using Monte Carlo or Latin hypercube sampling, this study uses a 3rd-order Gauss-Legendre quadrature. The quadrature is shown on the right side of Eq.2, where for the 3rd quadrature order I=2, $\mathbf{Y}(\mathbf{Z_i},x)$ is the DSMC output variable at location x, $\mathbf{Z_i}$ is the random variable abscissa, w_i is the quadrature weight that can be found in table 2 and $\rho(z_i)$ for the considered distribution is 1/2. Note that the Legendre polynomials are orthogonal only on the [-1,1] interval and Gauss-Legendre quadrature is applicable only on the [-1,1] interval. If the random variable studied, **Z**, is defined on a different interval then it needs to be rescaled to test random variable, z, using Eq. 3.

$$y(z,x) = a_0(x)\psi_0(z) + a_1(x)\psi_1(z) + a_2(x)\psi_2(z) + \ldots + a_N(x)\psi_N(z) \tag{1}$$

$$a_n(x) = \frac{< y(z,x)\psi(z) >}{< \psi_n^2(z) >} = \frac{1}{\int_{-1}^{1} \left(\psi_n^2(z)\rho(z)dz\right)} \sum_{i=0}^{I} \left(\mathbf{Y}(\mathbf{Z}_i, x)\psi_n(z_i)\rho(z_i)w_i\right) \tag{2}$$

$$z = 2\frac{\mathbf{Z} - \mathbf{Z}_{\min}}{\mathbf{Z}_{\max} - \mathbf{Z}_{\min}} - 1 \tag{3}$$

TABLE (1). 3rd order Legendre Polynomials and Gauss-Legendre Quadrature

n,i	$\psi_n(z)$	$< \psi_n^2(z) >$	**Abscissas** z_i	**Abscissas** $\mathbf{Z_i}$	**Weights** w_i
0	1	1	$-\sqrt{\frac{3}{5}}$	$\bar{\mathbf{Z}} - \frac{(\mathbf{Z}_{\max} - \mathbf{Z}_{\min})}{2}\sqrt{\frac{3}{5}}$	5/9
1	z	1/3	0	$\bar{\mathbf{Z}}$	8/9
2	1/2 ($3z^2$-1)	1/5	$\sqrt{\frac{3}{5}}$	$\bar{\mathbf{Z}} + \frac{(\mathbf{Z}_{\max} - \mathbf{Z}_{\min})}{2}\sqrt{\frac{3}{5}}$	5/9

The mean, shown in Eq. 4 can be computed by taking the expectation of Eq.1 and realizing that the 2nd and 3rd terms become zero. Standard deviation, σ, can also be computed from Eq.1 and be simplified to Eq.5.

$$\bar{y}(x) = < y(z,x) > = a_0(x) \tag{4}$$

$$\sigma(x) = \sqrt{< (y(z,x) - \bar{y}(x))^2 >} = \sqrt{\sum_{n=1}^{2} a_n^2(x) < \Psi_n^2(z) >} \tag{5}$$

The analysis is performed on a flat plate at Mach 10 in pure nitrogen. The freestream equilibrium conditions are summarized in table 2.

TABLE (2). Flow Conditions

Property	**Free Stream Value**
Fluid	Nitrogen
Velocity	1400 m/s (Mach 10)
Temperature (Trans, Vib, Rot)	47 K
Mean Free Path	0.0085 m
Pressure	6.57E-2 Pa
Density	4.6E-5 kg/m^3
Flat plate length	0.85 m (100 MFP)

Two gas-surface interaction input parameters that are of particular interest are surface temperature (T_w) and the tangential momentum accommodation coefficient (α_t). The accommodation coefficient is the ratio of specular to diffuse molecular reflections. The uncertainty in the accommodation coefficient is expected to be large because it depends on surface properties - surface finish, temperature, chemistry - and molecular gas properties. Note that the

surface material properties and temperature are likely to vary during a hypersonic flight. Uniform distribution profiles are used for surface temperature and the accommodation coefficient. The accommodation coefficient is varied from 0.5 to 1, which is equivalent to an input uncertainty of 19%. Measurements made by Ramesh show that the accommodation coefficient of stainless steel and nickel in nitrogen fall in this range [8]. The surface temperature is varied from 270K to 330K, which is equivalent to a 6 % uncertainty. Input and output uncertainties are defined as the standard deviation to mean ratio. The studied uncertainties are summarized in table 3. **Z** in Eq. 2 are T_w or α_τ

TABLE (3). Surface Model Uncertainties

Property	Mean ($\bar{\mathbf{Z}}$)	Distribution (ρ)	Range ($\mathbf{Z}_{max} - \mathbf{Z}_{min}$)	Variation	Uncertainty
Surface Temperature	300 K	Uniform	270-330 K	10 %	6 %
Accommodation Coefficient	0.75	Uniform	0.5 - 1.0	33 %	19 %

NUMERICAL APPROACH AND VERIFICATION

Uncertainty analysis is performed on the flowfields and surface solutions obtained with the DSMC SMILE code [9]. The collision domain with 260 by 60 cells that span 1.105 m by 0.255 m in physical space is used in this analysis. The initial size of the collision cell is half of the mean free path but can be divided up to 10 times if local mean free path decreases. SMILE samples the collision domain for 200,000 time steps before generating flowfield and surface solutions. Monte Carlo sampling in SMILE results in a sampling uncertainty that scales approximately as $1/\sqrt{N}$, where N is the number of samples. To quantify sampling uncertainty, solutions sampled for 200,000 time steps are compared to those sampled for 800,000 time steps. Flowfield temperature and density of the two sampling solutions differ by less than 2%, while surface friction, normal stress and heat flux differ by less than 1%.

Doubling the computational and physical domains in the downstream direction results in less than 3% point variation in the flowfield temperature and density but less than 1% variation in the surface parameters. Therefore, uncertainties computed by gPC of less than 5% in the flowfield and less than 3% on the surface are considered insignificant.

Weaver et al [5] showed that a third-order gPC can accurately reproduce the first two moments of the stagnation point heat transfer for high Mach flows. Moving to a fourth-order gPC changed the mean heat flux by less than 0.1%. Third order gPC solution also deviated by less than 0.1% from a random Monte Carlo solution with ten million sampling points. Hence, the third-order gPC analysis is sufficient and has been applied in this work.

RESULTS AND DISCUSSION

The effect of the accommodation coefficient uncertainty on the hypersonic flow over a flat plate is studied first. The accommodation coefficient is varied uniformly between 0.5 and 1.0, which corresponds to a 19% uncertainty. The resultant averaged temperature flowfield is presented in Fig. 1a while temperature uncertainty due to the accommodation coefficient variation is presented in Fig. 2a. Averaged flowfields are obtained from three DSMC runs in which only the accommodation coefficient is changed. In the studied case the temperature reaches a maximum value of 567K and a maximum uncertainty of 19 %. Flowfield temperature uncertainty first develops in the shock-boundary layer interaction region and convects downstream in two bands. Along the surface, temperature uncertainty drops to just 5 % away from the shock-boundary layer interaction zone. The maximum output flowfield temperature uncertainty is equivalent to the input accommodation coefficient uncertainty.

Averaged density flowfield and density uncertainty due to the accommodation coefficient are shown in Fig. 1b and 2b respectively. Density increases along the shock to a maximum value of 9.4E-6 kg/m^3 and decreases along the plate to a minimum value of 2.3E-6 kg/m^3. Density is lower near the plate because flowfield temperature is higher there and the flow is turned away from the plate by the shock. The density uncertainty also increases along the shock and a maximum uncertainty of 24 % is found where the density is highest. Along the surface, density uncertainty remains below 5%. Interestingly, a 10% uncertainty region exists between the shock and the surface.

Surface temperature (T_w) averaged flowfields are similar to accommodation coefficient averaged flowfields. Flowfield temperature uncertainty due to surface temperature is distributed nearly uniformly below the shock and remains below 3%. The density uncertainty profile due to surface temperature variation is similar to the density uncertainty profile presented in Fig. 2b but attains a maximum value of just 3%. These uncertainties are considered insignificant because they are smaller than the numerical uncertainties and input T_w uncertainty. Due to space constraints these flowfield plots are not presented in this paper.

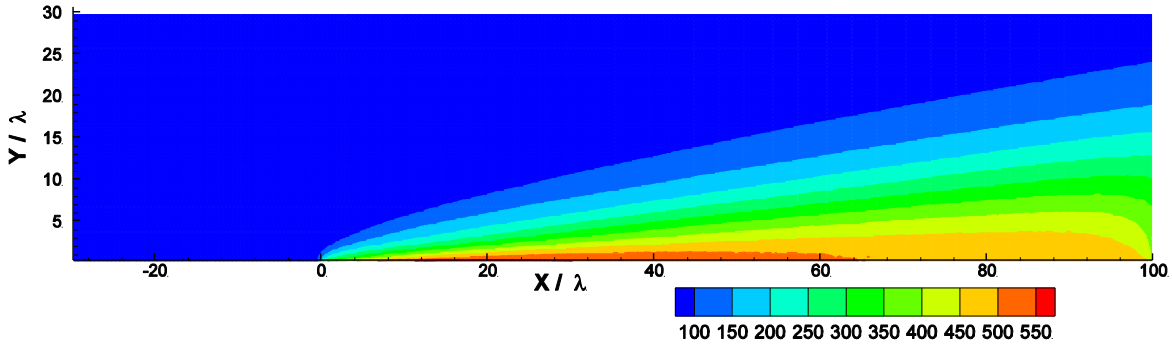

a) Mean temperature flowfield (K)

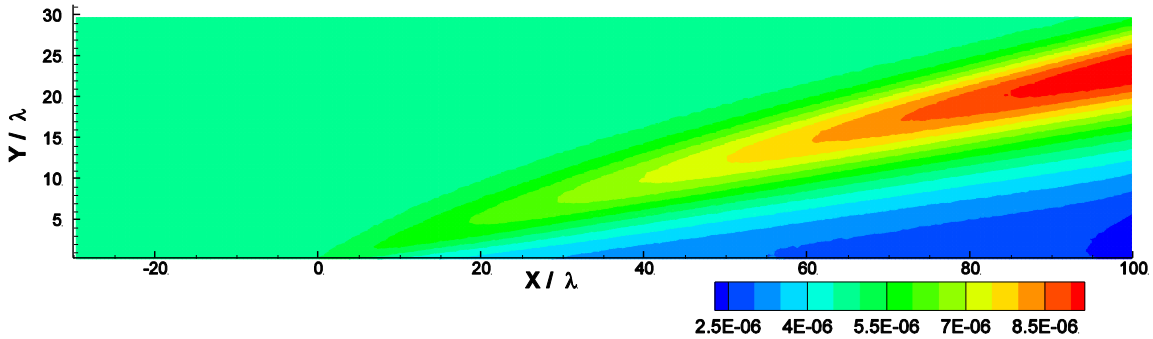

b) Mean Density Flowfield (kg/m^3)

FIGURE 1. Average temperature and density flowfields with a 0.75 mean accommodation coefficient and a 19 % uncertainty.

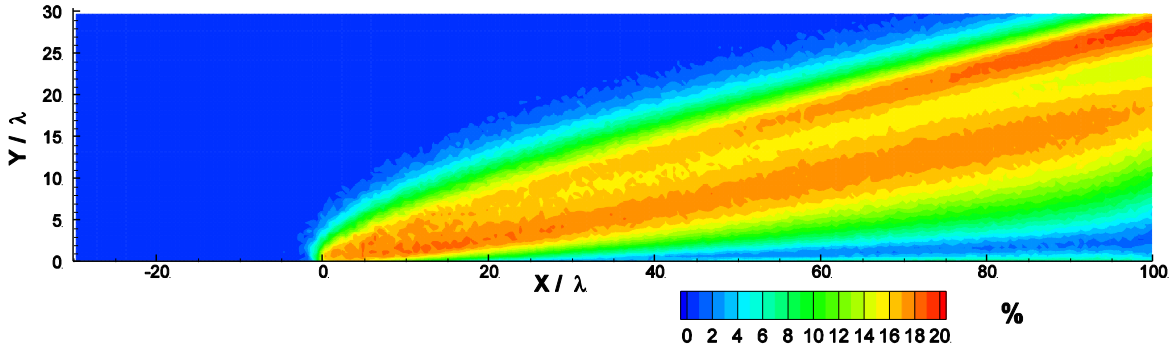

a) Flowfield temperature uncertainty due to the accommodation coefficient

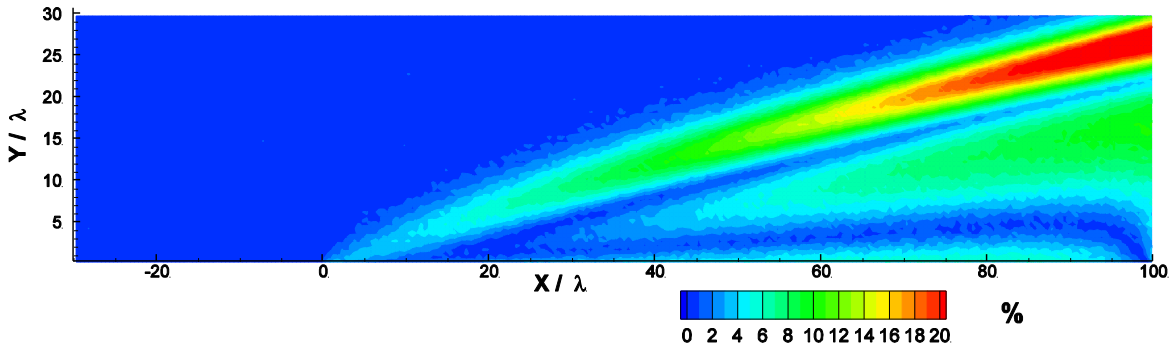

b) Flowfield density uncertainty due to the accommodation coefficient

FIGURE 2. Temperature and density flowfield uncertainty due to a 19 % accommodation coefficient uncertainty.

Mean shear stress, heat flux and normal stress are presented in figures 3a, 3b and 3c respectively. Accommodation coefficient averaged profiles are obtained from three DSMC runs in which only the accommodation coefficient is varied, while the surface temperature averaged profiles are obtained from three runs in which only the surface temperature is varied. The accommodation coefficient and surface temperature averaged profiles are similar but not equivalent. Shear stress is normalized by the dynamic head, heat flux is presented as a Stanton number and normal stress is normalized by upstream pressure. Shear stress and heat flux profiles attain a maximum value at 8 MFP from the leading edge, while normal stress attained a maximum value 28 MFP from the leading edge.

Shear stress, normal stress and heat flux uncertainty profiles due to the accommodation coefficient are presented in Fig. 4a. The three uncertainty profiles increase from the leading edge up to a maximum 4 MFP from the leading edge and then decrease again in the downstream direction. Shear stress, normal stress and heat flux have maximum uncertainties of 22%, 16% and 22% respectively. The shear stress and heat flux uncertainties are greater than the input accommodation coefficient uncertainty while the normal stress uncertainty is smaller. Surface uncertainties due to surface temperature variation, found in Fig. 4b, remain below 3% for the entire span of the plate and are considered insignificant.

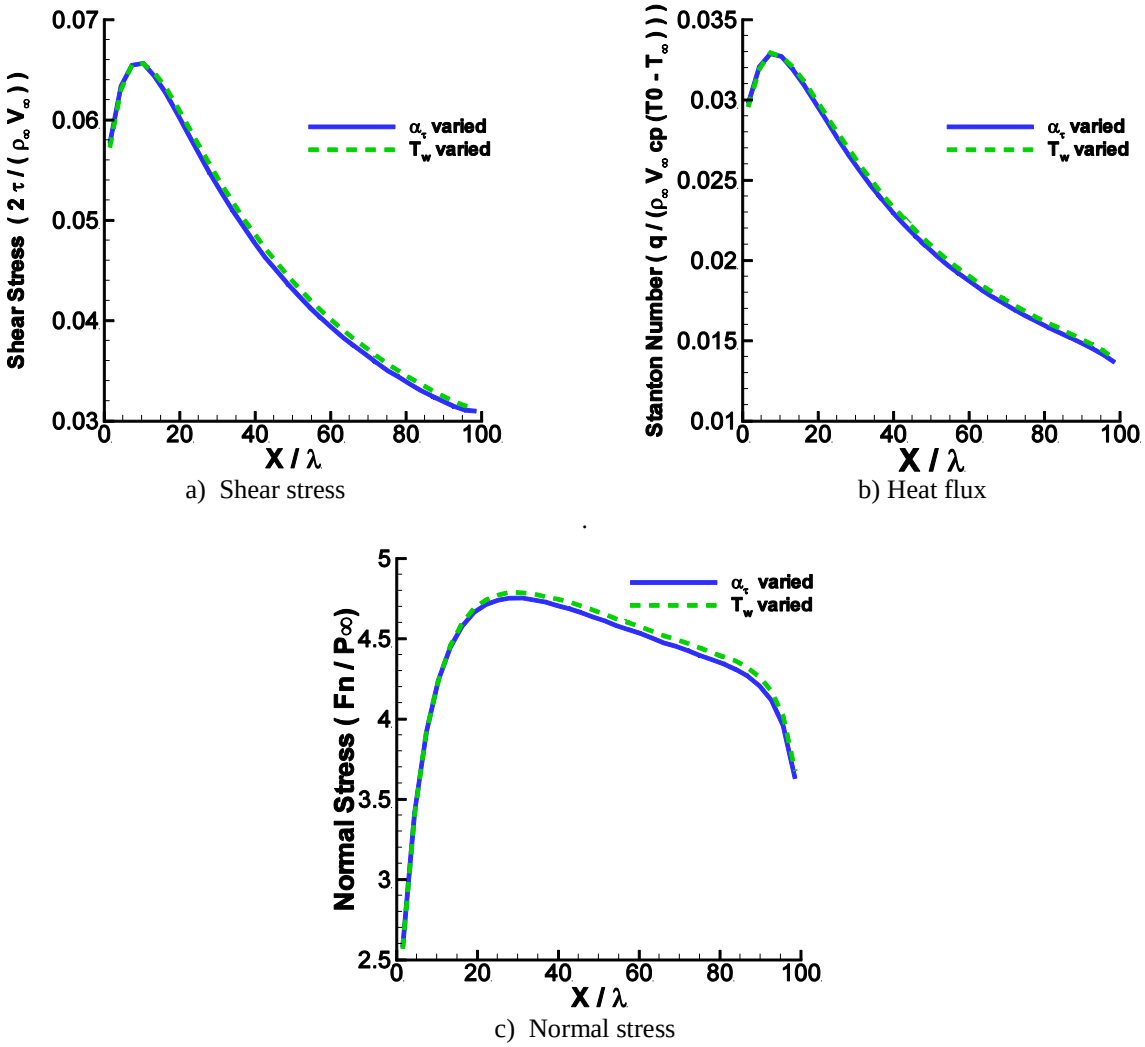

a) Shear stress

b) Heat flux

c) Normal stress

FIGURE 3. Accommodation coefficient (blue) and surface temperature (green) averaged shear stress, heat flux and normal stress. Averaged profiles were obtained by calculating the gPC mean profile from the three DSMC solutions.

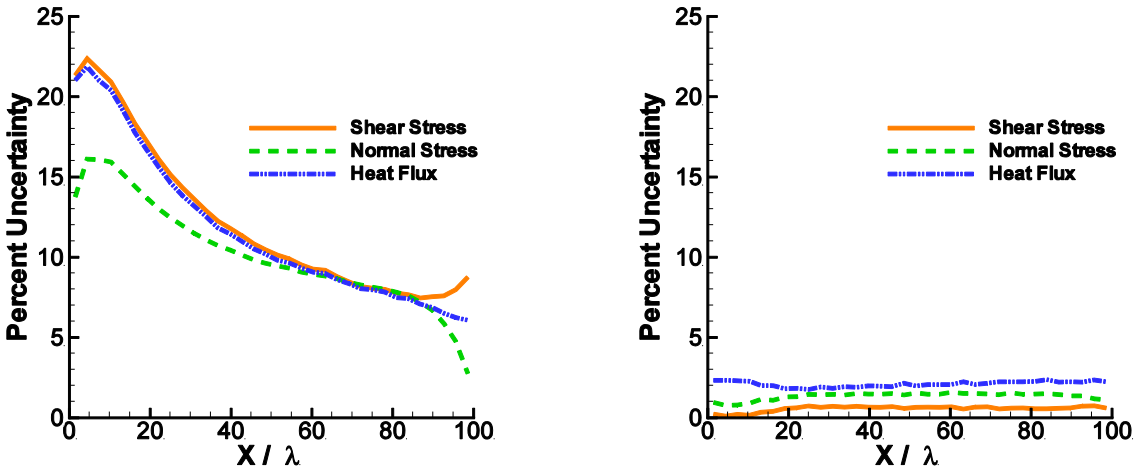

a) Uncertainty due to the accommodation coefficient b) Uncertainty due to the surface temperature

FIGURE 4. Surface shear stress, normal stress and heat flux uncertainty profiles.

CONCLUSIONS

A polynomial chaos method is used in this study to assess the effects of uncertainty in the gas-surface accommodation coefficient and wall temperature on the hypersonic boundary layer development near a sharp leading edge. Uncertainties in the flowfield temperature, flowfield density, surface shear, heat flux and normal stress are analyzed based on the DSMC calculations combined with polynomial chaos sampling of parameter space. The polynomial chaos method can produce accurate output PDFs based on just three DSMC flowfield samples. It is shown that the surface accommodation coefficient uncertainty is amplified in the vicinity of the leading edge and drops in the downstream direction along the surface, whereas the output uncertainties due to the wall temperature variations remains nearly constant along the surface and is below the input uncertainty everywhere. A 19% accommodation coefficient uncertainty can result in a 16% uncertainty in the normal stress, 22% uncertainty in the shear stress and heat flux. On the other hand, a 6% surface temperature uncertainty results in insignificant flowfield and surface flux uncertainties. Therefore, in order to increase confidence of aeroheating predictions for hypersonic sharp-leading edge configurations one needs to diminish uncertainty in the surface accommodation coefficient.

REFERENCES

1. J.J. Bertin, R.M. Cummings, "Critical Hypersonic Aerodynamic Phenomena", Annu. Rev. Fluid Mech., 38, pp. 129-157.
2. Bose, D., Wright, M., and Palmer, G., "Uncertainty Analysis of Laminar Aeroheating Predictions for Mars Entries," J. Thermophysics Heat Transfer, Vol. 20, No. 4, 2006, pp. 652.
3. Najm, H., "Uncertainty quantification and polynomial chaos techniques in computational fluid dynamics," *Annual Review of Fluid Mechanics*, Vol. 41, 2009, pp. 35–52.
4. Xiu, D. and Karniadakis, G., "Modeling uncertainty in flow simulations via generalized polynomial chaos," *Journal of Computational Physics*, Vol. 187, No. 1, 2003, pp. 137–167.
5. Balepin, V., Maita, M., and Murthy, S., "Third Way of Development of Single-Stage-to-Orbit Propulsion," *Journal of Propulsion and Power*, Vol. 16, No. 1, 2000, pp. 99–104.
6. Bird, G., *Molecular gas dynamics and the direct simulation of gas flows*, Clarendon Press Oxford, 2003.
7. Weaver, A., Alexeenko, A., R. Greendyke, J. Camberos, "Flowfield Uncertainty Analysis for Hypersonic CFD Simulations," AIAA Paper 2010-1180, 48th AIAA Aerospace Sciences Meeting, 2010.
8. V Ramesh and DJ Marsden, "Rotational and translational accommodation coefficients of nitrogen on nickel, silver and gold," *Vacuum*, Vol. 24, No. 7, pp. 291-294.
9. Ivanov, M., Kashkovsky, A., Gimelshein, S., Markelov, G., Alexeenko, A., Bondar YeA, Z., Nikiforov, S., and Vaschenkov, P., "SMILE System for 2D/3D DSMC Computations," Proceedings of 25th International Symposium on Rarefied Gas Dynamics, St. Petersburg, Russia, July, 2006, pp. 21–28.